Genes & Diseases

FULL LENGTH ARTICLE

Chinese herbal decoction astragalus and angelica exerts its therapeutic effect on renal interstitial fibrosis through the inhibition of MAPK, PI3K-Akt and TNF signaling pathways

Hao Yuan [a,b,†], Xuelian Wu [a,†], Xiaomin Wang [c], Chengfu Yuan [a,*]

[a] College of Medical Science, China Three Gorges University, Yichang, Hubei 443002, PR China
[b] BGI Education Center, University of Chinese Academy of Sciences, Shenzhen, Guangdong 518083, PR China
[c] Chumeiren Medical Cosmetic Clinic, WuJiaGang District, Yichang, Hubei 443002, PR China

Abstract Astragalus and Angelica decoction (A&A) has been clinically used as a classical traditional Chinese medicine (TCM) formula in China for many years for the treatment of kidney diseases, especially renal interstitial fibrosis (RIF). However, the mechanisms underlying the therapeutic effects of A&A on RIF remains poorly understood. In the present study, systematic network pharmacology and effective experimental verification were utilized for the first time to elucidate the pharmacological efficacy and potential mechanism. The outcomes indicated that 22 active components and 87 target genes of A&A were identified and cross-referenced with RIF-associated genes, contributing to confirmation of 74 target genes of A&A for RIF. Pathway and functional enrichment analyses revealed that A&A had substantial effects on MAPK, PI3K-Akt and TNF signaling pathways. In addition, seven core targets with relatively higher betweenness and degree were identified in the constructed Chinese medicine material-chemical component-target-signal pathway network. Moreover, we verified the potential therapeutic effect of A&A *in vivo* (using a mouse model of RIF), confirming that A&A could effectively protect the kidney by regulating these target genes. The therapeutic effect of A&A on RIF could be attributed to its role in regulating the cell cycle, limiting the apoptosis, and inhibiting the inflammation.

* Corresponding author. College of Medical Science, China Three Gorges University, Yichang, Hubei 443002, PR China. Fax: +86 717 6396818.
E-mail address: yuancf46@ctgu.edu.cn (C. Yuan).
Peer review under responsibility of Chongqing Medical University.
† These authors contributed equally to this work.

Introduction

Chronic kidney disease (CKD) has already become one of the significant public health threats worldwide,[1] and renal interstitial fibrosis (RIF) is a common pathologic manifestation of various CKDs.[2,3] Current research reveals that RIF results from excessive deposition of extracellular matrix (ECM) and interstitial fibroblast proliferation, which is involved in the alteration of multiple signaling pathways and biological processes.[4,5] Therefore, RIF is a typical progressive disease with multiple target genes, and it requires combinatorial drug intervention. The pathogenesis of RIF is a chronic process that the effective therapeutic choices for patients with end-stage renal disease are confined to dialysis and renal transplantation.[6] There is no currently available targeted therapy for RIF despite the fact that the etiology and symptoms of RIF have been extensively investigated. Currently, as the rate of RIF caused by renal disease is constantly increasing, it is urgently necessary to develop more effective anti-fibrotic therapeutic strategies.

Astragalus and Angelica decoction (A&A), a traditional Chinese medicine (TCM) formula named "Huangqi Danggui Tang" in Chinese, is mainly made from Astragalus membranaceus and Angelica Sinensis. These two herbal medicines have been used for the treatment of anemia, chronic cardiovascular disease and chronic inflammatory disease, as recorded by ancient Chinese pharmacopoeias.[7] Astragalus, when used alone or in combination with Angelica, has been reported to have a good clinical activity with CKD.[8,9] Meanwhile, A&A have a renoprotective effect in animal models, including ischemia-reperfusion injury[10] and chronic puromycin aminonucleoside nephrosis,[11] exhibiting improved renal microvascular function and ameliorated interstitial fibrosis.[12,13] However, the molecular mechanism underlying the therapeutic effect of A&A still remains largely unexplored.

Network pharmacology has been cited and developed as a promising approach for the study of TCM since its proposal in 2010.[14] Based on an approach of "multi-gene-multi-target-complex disease" that systematically explores the interaction of target genes, compounds, herbs and diseases, we applied the network pharmacology approach to explore the pharmacological properties, mechanisms of A&A against RIF.

First, chemical components of A&A, including Astragalus and Angelica, were retrieved from Traditional Chinese Medicine Systems Pharmacology (TCMSP) database. Moreover, active compounds with high oral bio-availability (OB) and drug-likeness (DL) scores were selected.[15] Secondly, target genes of active compounds were cross-referenced with target genes of potential disease via two databases (DisGeNET and Genecards) to identify potential targets of A&A. Subsequently, the potential mechanism of A&A against RIF was identified by Gene Ontology (GO) and Kyoto Encyclopedia of Genes and Genomes (KEGG). Meanwhile, Chinese medicine material-chemical component-target-signal pathway network was established based on the target genes with Cytoscape, from which TP53, RELA, CCND1, RAF1, CASP3, CASP9 and GSK-3β were found as target genes that might play an important role in therapy for RIF. In addition, the RIF animal model was used to verify the pharmacological mechanism of A&A. Collectively, our findings enhanced in-depth understanding of A&A, making it beneficial to more people.

Materials and methods

Collected chemical components of each herb in A&A

Chemical components in A&A were retrieved from TCMSP database.[16] A total of 22 compounds were collected in A&A, including 20 compounds in Astragalus and two compounds in Angelica. Several components were found in more than one herb.

Screening of disease-drug target genes

Chemical properties of compounds of A&A were obtained from the TCMSP database. The molecular properties mainly included octanol–water partition coefficient (ALogP), DL, molecular weight (MW) and OB. These features have been confirmed as core chemical properties of drugs.[16] In these properties, OB is the percentage of oral dose that enters systemic circulation.[17] DL is a qualitative concept evaluating the structural similarity in drug design, which was conducted to optimize pharmaceutical properties, such as chemical stability and solubility.[18] On the one hand, putative targets of selected components were obtained only if both OB ≥ 30%[17] and DL ≥ 0.18[19] in TCMSP database, and redundancy with no target genes was removed. On the other hand, target genes of potential disease were obtained from databases of Genecards[20] (https://www.genecards.org/) and DisGeNET[21] (http://www.DisGeNET.org/). The two subsets of the targets obtained from A&A pharmacological genes and pathogenic genes of RIF were cross-referenced to deduce the potential disease-drug target genes. Venn diagrams were used to determine the intersection of the two subsets.

Pathway and functional enrichment analysis

To understand the potential biological implications of disease-drug target genes, enrichment analysis with GO terms and KEGG pathways was performed using the clusterProfiler package[22] in R.

Construction of the network

Based on the prediction of potential target genes of A&A against RIF, Chinese medicine material-chemical component-target-signal pathway network was established using Cytoscape3.7.2 software. Degree, betweenness centrality and network centralization were good indicators of target genes' centrality within a network. Nodes in the network that were connected with edges represented Chinese medicine material, chemical component, target genes and signal pathway.

Experimental verification of network pharmacology with animal RIF model

Preparation of an oral decoction of A&A

Astragalus is the dry root of *Astragalus membranaceus* var. *mongholicus*, which is originated from the Shanxi Province, China. Angelica is the dry root of *Angelica sinensis*, which is originated from the Gansu Province, China. Prof. Chengfu Yuan's group, College of Medical Science, Three Gorges University, China, has accomplished the identification of the botanical origin of these two herbs, as well as the preparation and quality control of A&A. According to the previously described preparation method,[11] equal amounts of Astragalus and Angelica were chopped and put into a leacher, followed by extraction for three times using the water reflux method. Next, eight volumes of water were added and boiled for 2 h, and the water extract was obtained after being cooled. Subsequently, six volumes of water were added to the extract, the mixture was boiled for 1 h, followed by extraction, and such procedure was repeated twice. Finally, all of the extracts were pooled, filtered and condensed using a vacuum at 60 °C, and the final concentration of the decoction named as "A&A" in this paper was 0.7 g/mL for each herb. Next, 0.1% of sodium benzoate was added, and the concentrate was sub-packaged and stored at −4 °C.

A reliably and reproducible chemical composition of A&A is a prerequisite for exerting the biological effects of this Chinese medicine preparation. Calycosin glycoside, calycosin, formononetin and astragaloside IV are the characteristic components of Astragalus; and ferulic acid is the characteristic component of Angelica.[23,24] In the previous research, Xu et al have verified the reproducibility of the major constituents of A&A, including above-mentioned components, using high-performance liquid chromatography.[25,26]

Experimental animals

A total of 40 male C57BL/6J mice, weighing 18−22 g, SPF level, were purchased from Beijing Vital River Laboratory Animal Technology Co., Ltd. The animal certificate was No. SCXK (Beijing) 2016-0006. Mice were bred at the experimental animal center of Three Gorges University at a constant temperature of 20 ± 2 °C and a humidity of 55 ± 5%. All animals were adaptively bred for 1 week before the experiment.

Establishment of RIF model and drug administration

Mice were randomly and evenly divided into four groups, namely sham-operation group (sham group), unilateral ureteric obstruction group (UUO group), low-dose A&A group (A&A-L group) and high-dose A&A group (A&A-H group). UUO group, A&A-L group and A&A-H group underwent left ureteral ligation under sterile conditions. The sham group was subjected to the same surgical procedure. After the first day of operation, the mice in the A&A-L group and A&A-H group were given 0.5 mL A&A decoction by gavage every day. Simultaneously, the mice in the sham group and UUO group were given same volume of saline by gavage once a day. At 21 days after the operation, venous blood was taken from the venous sinus, which was allowed to stand for 1 h before centrifugation at 3,000 rpm for 10 min. The serum was collected and stored at −20 °C for the determination of serum creatinine (SCr) and blood urea nitrogen (BUN) contents. The mice were sacrificed by carbon dioxide asphyxiation, and the left kidney was dissected. A portion was fixed in 4% paraformaldehyde for Masson staining, and the other portion was stored at −80 °C for molecular biology experiments.

Evaluation of serum BUN and SCr

Serum BUN and SCr levels were determined according to the instructions of the commercial kits.

Pathological observation

The kidney tissues were rinsed with saline, and the surface water was sucked with filter paper. Then the kidney tissues were fixed in 4% paraformaldehyde, embedded in paraffin and cut into 4-μm sections. Each section was visualized under a light microscope to evaluate the state of collagen deposition in the kidney after Masson staining. Quantitative analysis was assessed using IMAGE PRO Plus 6.0 software. Moreover, 10 different visual fields were randomly selected from each slice by optical microscopy (200× magnification). The area with blue fiber was positive, and the ratio of the positive area to the total area of the visual field was used as the renal fibrosis index.

Quantitative real-time PCR

Total RNA was isolated from mouse kidney tissues using TRizol reagent. Purified RNA was reversely transcribed into cDNA. qRT-PCR was performed with the SYBR Green Master Mix kit (Qiagen Corporation). Briefly, after an initial denaturation step at 95 °C for 10 min, amplifications were carried out with 40 cycles at a melting temperature of 95 °C for 15 s, and an annealing temperature of 60 °C for 60 s. Relative expressions of target genes were calculated using the $2^{-\Delta\Delta Ct}$ method, while GAPDH was selected as housekeeping gene. Sequences of the primers used in the present study were shown in Table S1.

Western blotting analysis

Kidney tissues were lysed in radioimmunoprecipitation assay (RIPA) buffer supplemented with 100 mmol/L PMSF and ground into fragments at low temperature. Subsequently, the homogenate was centrifuged at 12,000 rpm for

10 min at 4 °C, and supernatant was collected. The protein concentration was determined by the BCA protein kit. Briefly, equal amounts of proteins were subjected to sodium dodecyl sulfate (SDS) polyacrylamide gel electrophoresis, and then transferred onto PVDF membrane. The membrane was blocked with 5% skim milk for 2 h, followed by incubation with primary antibodies at 4 °C overnight. The membranes were washed with TBST for five times (5 min for each), followed by incubation with the corresponding horseradish peroxidase-labeled secondary antibody for 2 h. Finally, the membranes were washed, and immunoreactive bands were visualized with enhanced chemiluminescence (ECL) reagent kit.

Immunohistochemistry

The renal tissue sections from histopathologic evaluation were also used for immunohistochemical analysis. Kidney sections (4 μm) were subjected to xylene dewaxing, gradient alcohol rehydration, and antigen retrieval with 0.01 M citrate buffer (pH 6.0). Then the endogenous peroxide activity was blocked with 3% H_2O_2 and 5% bovine serum albumin (BSA) at 25 °C. Subsequently, the sections were incubated with antibodies against NFκB p65 (1:100) and p53 (1:100) overnight at 4 °C. The slides were then washed with PBS and incubated with the corresponding secondary antibodies for 1 h. After strained with diaminobenzidine, the slides were counterstained with hematoxylin, differentiated with hydrochloric acid alcohol, dehydrated with gradient ethanol, and transparentized with xylene. Finally, the positive expression of tan was visualized under the microscope. A total of 10 different visual fields were randomly selected in each section, and the relative positive staining area was acquired by Image Pro Plus 6.0.

Statistical analysis

All experimental data were processed using SPSS 13.0 software, expressed as mean ± standard deviation, and statistically analyzed by variance and t-test. GraphPad Prism 7 software was used for drawing graphs of related statistical analyses.

Results

Identification of active compounds and targets of A&A

The components of two herbs in A&A were collected from the TCMSP database. There were 22 active compounds identified from the two herbs of the A&A (Table S2). Moreover, 462 corresponding target proteins were identified from these 20 active compounds in Astragalus. In addition, two active compounds targeting 69 proteins were identified from Angelica. A total of 531 target proteins and 87 target genes in A&A were obtained (Table S3). Figure 1 shows the chemical component-target network. The components and potential targets of Astragalus and Angelica, which constitutes A&A, were identified and shown in Table 1. A total of 4,433 target (Table S4) genes of RIF were identified from the Genecards database and DisGeNET database. Figure 2A shows that target genes identified from

the two databases with the potential targets of A&A indicated 74 cross disease-drug targets.

Gene function annotation analysis of potential targets of A&A

The enrichment analysis of 74 putative targets was conducted using the clusterProfiler package. This package realized the methods to analyze and visualize functional profiles (GO terms and KEGG pathways) of genes. Fig. 2B depicts the GO enrichment analysis (Table S5), including reactive oxygen species metabolic process, receptor complex, transcription factor binding and so on. Moreover, KEGG pathway enrichment analysis (Table S6) indicated that A&A exerted its protective effort. Fig. 2C reveals that many significant signaling pathways played a critical role in A&A-treated renal fibrosis, including PI3K-Akt signaling pathway, HIF-1 signaling pathway and mitogen-activated protein kinase (MAPK) signaling pathway. Figure 2D lists the detailed information about the relationship between target genes and KEGG terms in A&A.

Construction of the Chinese medicine material-chemical component-target-signal pathway network

Cytoscape 3.7.2 software was used to construct the network, which was composed of 124 nodes (two Chinese medicines, 18 compounds, 30 signaling pathways, and 74 targets) and 565 edges. Based on the network analysis, the network topology showed a high level of interconnectivity, from which the network heterogeneity and centralization were scored as 0.857 and 0.429, respectively. More attention should be paid to the degree and betweenness. The number of connections of that node with other nodes was the degree of a node. Moreover, the proportion of the shortest path through the node to the total path was the betweenness. With the increased degree and betweenness, the node became more and more important. Figure 3 shows that the target genes TP53 (betweenness: 0.035966; degree: 26), RELA (betweenness: 0.042635; degree: 24), CCND1 (betweenness: 0.025234; degree: 22), RAF1 (betweenness: 0.02528; degree: 22), CASP3 (betweenness: 0.03157; degree: 21), CASP9 (betweenness: 0.020981; degree: 18) and GSK-3β (betweenness: 0.03699; degree: 18) had higher median values and degrees, indicating that they were potential core targets of A&A in the treatment of RIF.

Comparison of renal function between different groups

Compared with the sham group, the serum BUN and SCr levels of the UUO group were significantly increased after modeling, and there was statistically significant difference between the two groups ($P < 0.01$). Compared with the UUO group, the serum BUN and SCr levels of the A&A-L group and A&A-H group were decreased to varying degrees, especially in the high-dose group, and the difference was statistically significant ($P < 0.05$). The result was shown in Figure 4A and Figure 4B.
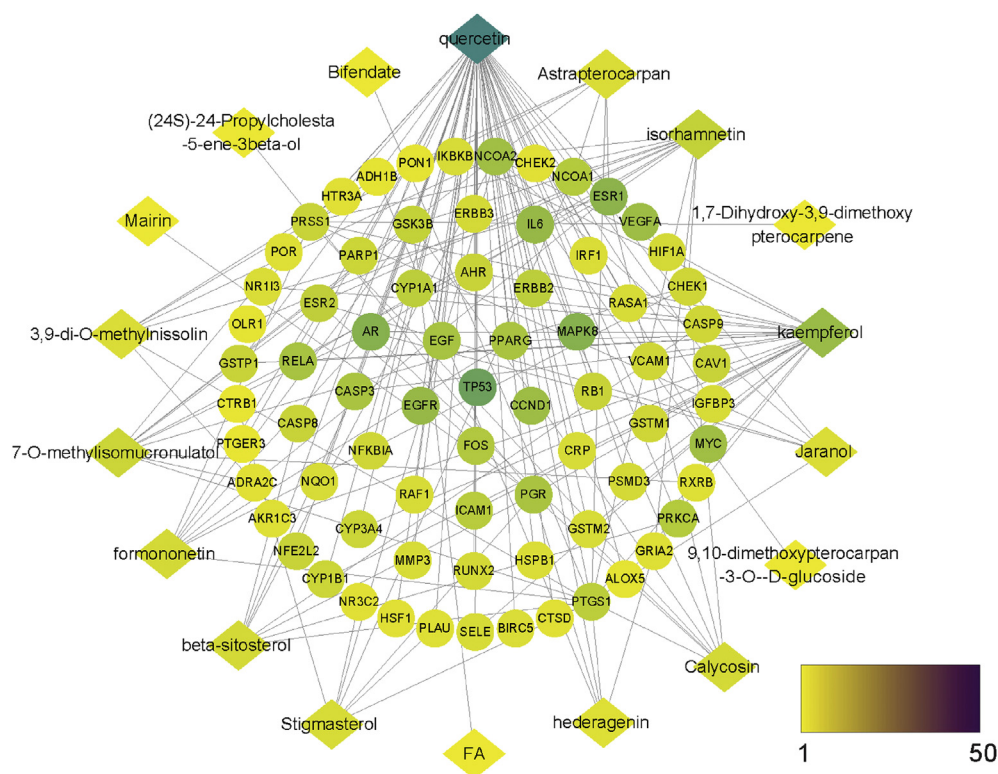
Figure 1 Component-target network diagram. The diamond node represents compound in A&A. The oval node represents the target. Different colors represent the degree, as the scale indicates.
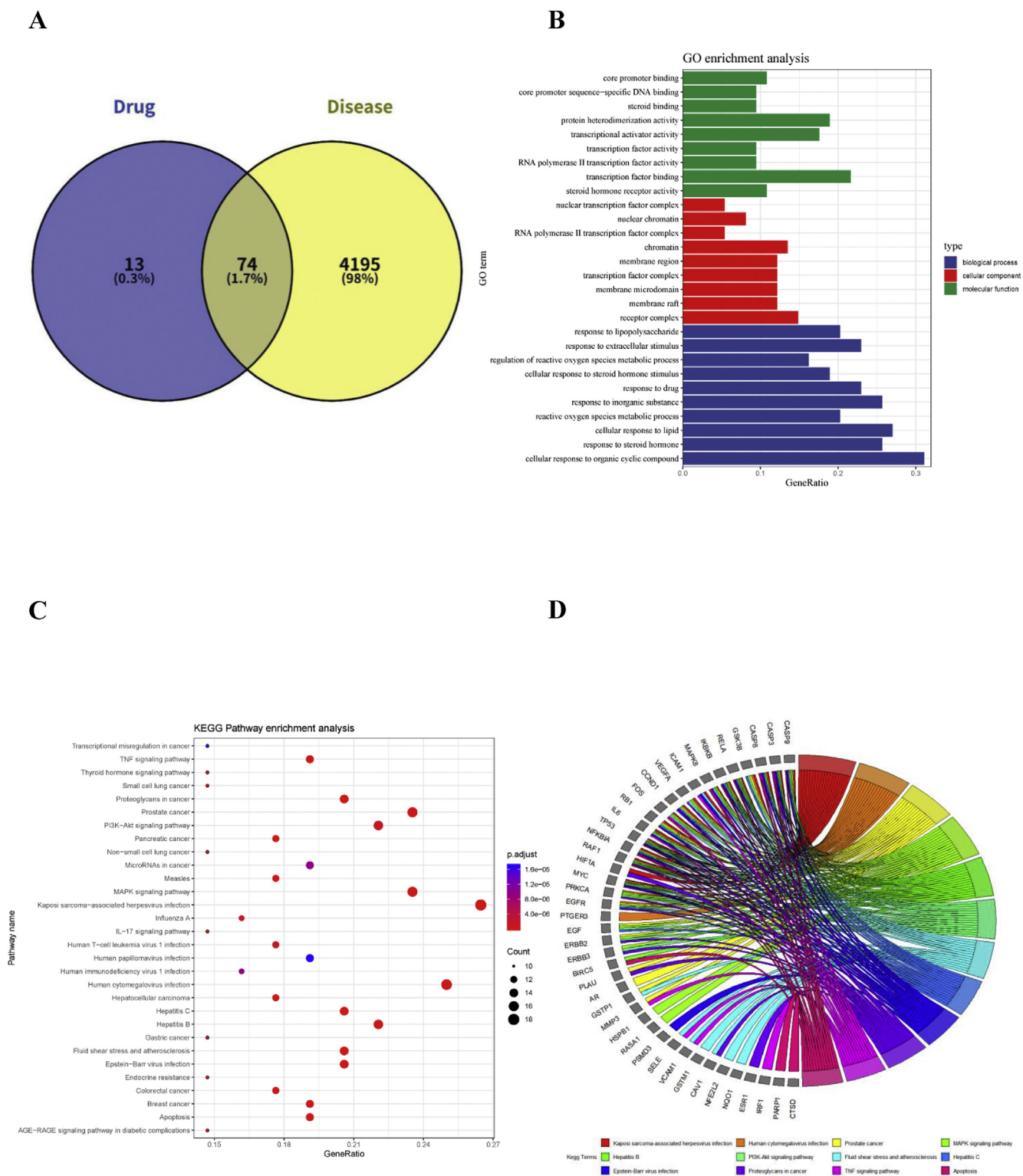
Table 1 Component and target of A&A.

Herb	Component	Target
Angelica	Beta-sitosterol, stigmasterol	PGR,NCOA2,PTGS1,ADRA1A,CHRNA2,GABRA1,CASP9, CASP3,CASP8,PRKCA,PON1,NR3C2,NCOA1,PLAU,CTRB1,
Astragalus	Mairin, jaranol, hederagenin,7-O-methylisomucronulatol, (24S)-24-Propylcholesta-5-ene-3β-ol, isorhamnetin, 3,9-di-O-methylnissolin, 5′-hydroxyiso-muronulatol-2′, 5′-di-O-glucoside, isomucronulatol-7,2′-di-O-glucosiole, 9,10-dimethoxypterocarpan-3-O-β-D-glucoside, fulvic acids (FA), astrapterocarpan, bifendate, formononetin, isoflavanone, calycosin, kaempferol, quercetin, 1,7-Dihydroxy-3,9-dimethoxypterocarpene, (3R)-3-(2-hydroxy-3,4-dimethoxyphenyl)chroman-7-ol	PGR,PTGS1,AR,ESR2,CHEK1,PRSS1,NCOA2,GABRA1, GRIA2,ADH1B,ESR1,GSK3B,NCOA1,F7,ACHE,RELA,OLR1, HTR3A,ADRA2C,ADRA1A,RXRB,PPARG,IKBKB,AHSA1, CASP3,MAPK8,CYP3A4,CYP1A1,ICAM1,SELE,VCAM1, CYP1B1,ALOX5,GSTP1,AHR,PSMD3,NR1I3,DIO1,GSTM1, GSTM2,AKR1C3,MMP3,EGFR,VEGFA,CCND1,FOS,EIF6, CASP9,PLAU,EGF,RB1,IL6,TP53,NFKBIA,POR,CASP8,RAF1, PRKCA,HIF1A,RUNX1T1,ERBB2,ACACA,CAV1,MYC, PTGER3,BIRC5,DUOX2,HSPB1,NFE2L2,NQO1,PARP1, DCAF5,CHEK2,HSF1,CRP,RUNX2,CTSD,IGFBP3,IRF1, ERBB3,PON1,NPEPPS,HK2,RASA1

Abbreviations: A&A, astragalus and angelica decoction; TCM, traditional Chinese medicine; RIF, renal interstitial fibrosis; MAPK, mitogen-activated protein kinases; PI3K, phosphatidylinositol 3-kinase; AKT, protein kinase B; TNF, tumor necrosis factor.

Histopathological features

Masson staining results showed that the morphology and structure of kidney were normal in the sham group, and only a small amount of blue collagen and fibrin was positively stained between the tubules. In the UUO group, the aniline blue staining substance of tubulointerstitial tissue on the ligated side was significantly increased, the renal pelvis was severely dilated, renal tubules had severe degeneration and necrosis, RIF area was considerably accompanied by a large number of infiltrated inflammatory cells, RIF area was significantly increased, and the difference was statistically significant compared with the sham group ($P < 0.01$). Compared with the UUO group, the degree of renal fibrosis in the A&A-L group and A&A-H group was reduced, and the effect in the A&A-H group was more significant, with a significant difference ($P < 0.05$). The results were shown in Fig. 4C, D.
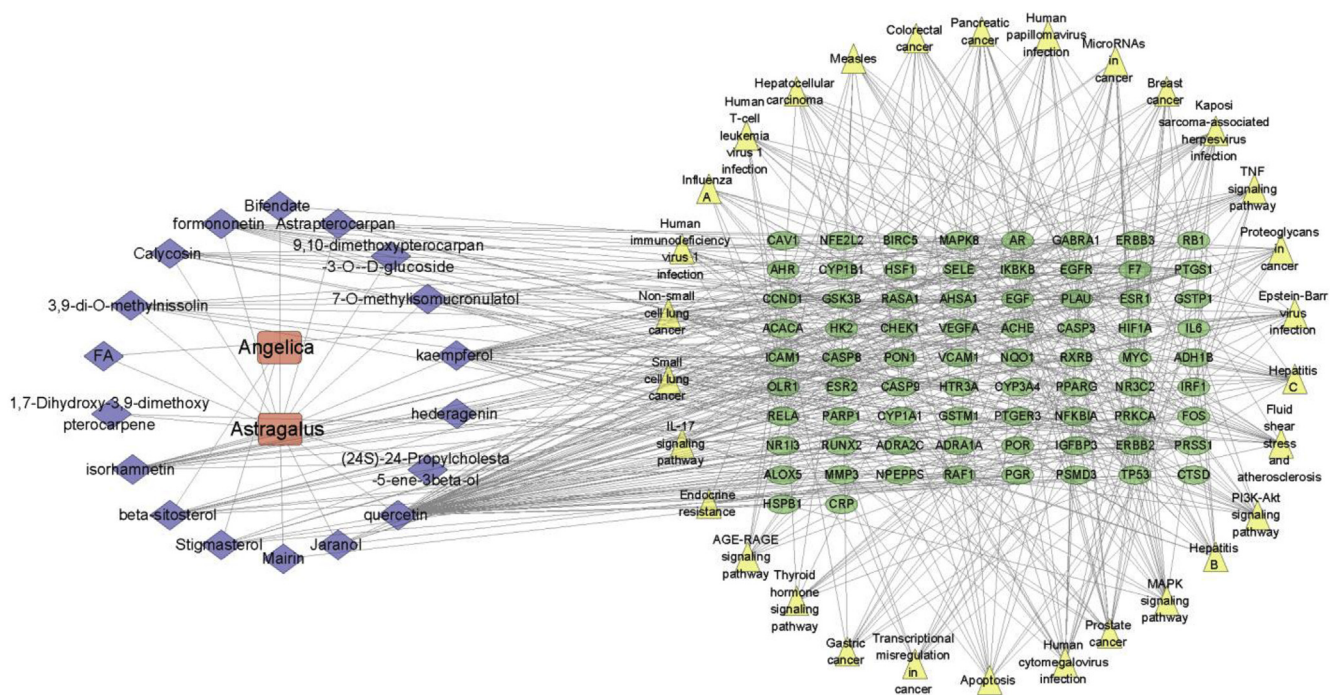
Figure 2 Venn diagram and functional analysis. (**A**) The intersection of disease targets and candidate targets in A&A. (**B**) GO enrichment entries in the top 10. (**C**) KEGG pathway enrichment entries in the top 30. (**D**) The complicated relationship between target genes and KEGG terms in A&A.

Figure 3 Chinese medicine material-chemical component-target-signal pathway network diagram. The round rectangle shape represents two Chinese herbal medicines; the diamond represents the chemical composition; the oval represents the target; and the triangle represents the signal path.

The effects of A&A on the expressions of P53, GSK3β, CCND1, Caspase 9, Caspase 3, and Raf1 at the mRNA and protein levels in renal tissue

Figure 5 shows that the expressions of P53, GSK3β, CCND1, Caspase 9, Caspase 3 and Raf1 at the mRNA level in the UUO group were significantly increased compared with the sham group ($P < 0.01$). However, the expressions of P53, GSK3β, CCND1, Caspase 9, Caspase 3 and Raf1 at the mRNA level in the A&A-L and A&A-H groups were decreased compared with the UUO group, especially in the A&A-H group ($P < 0.05$) (Fig. 5A). The representative results of above-mentioned findings were shown in Figure 5B (the experiment was repeated three times with the same trend).

Immunohistochemical analysis for the expressions of Raf1 and P53

Compared with the sham group, the expressions of both Raf1 and P53 were significantly increased in the UUO group ($P < 0.05$). Furthermore, lower levels of Raf1 and P53 were found in the A&A-L and A&A-H groups compared with the UUO group ($P < 0.05$). This finding suggested that A&A down-regulated the expressions of Raf1 and P53. The results were shown in Figure 6.

Discussion

As a TCM formula, A&A has a therapeutic effect on CKD, especially RIF. The present study suggested that 74 potential target genes were identified from active compounds of A&A using TCMSP database. Most of the compounds have both anti-inflammatory and anti-fibrotic properties, such as beta-sitosterol, stigmasterol,[27−29] hederagenin,[30] isorhamnetin,[31] astrapterocarpan,[32] formononetin,[33] calycosin,[34] kaempferol,[35] quercetin[36] and fulvic acids (FA).[37] Beta-sitosterol, stigmasterol, isorhamnetin, calycosin and quercetin down-regulate nuclear transcription factor nuclear factor κB (NF-κB) signaling,[27,29,31,34,36] while hederagenin, astrapterocarpan and FA modulate PI3K/AKT and MAPK signaling pathways.[30,32,37] To evaluate the association between these 22 compounds and RIF, we analyzed target genes acquired by cross-referencing compound targets and RIF related targets by GO terms and KEGG pathways, suggesting that its action mechanisms were primarily related to the MAPK signaling pathway, PI3K-Akt signaling pathway and TNF signaling pathway.

MAPKs, mainly p38 and ERK1/2, are involved in both acute kidney injury and progress of kidney disease, including RIF. It has also been demonstrated that MAPKs induce the transition of tubular epithelial cells into myofibroblasts through epithelial—mesenchymal transition (EMT). Furthermore, previous studies have identified activated MAPK as a physiologic activator of NF-κB, which participates in RIF and kidney damage.[38] Akt regulates multiple cellular processes, including growth, metabolism, proliferation and angiogenesis, with Akt phosphorylation at two sites (Thr308 and Ser473) via a PI3K-dependent process.[39] In the previous study, the PI3K inhibitor LY294002 has been reported to reduce the fibroblast proliferation and accumulation of ECM after UUO.[40] In addition, down-regulation of the PI3K/Akt signaling pathway not only suppresses EMT-associated α-SMA expression to promote
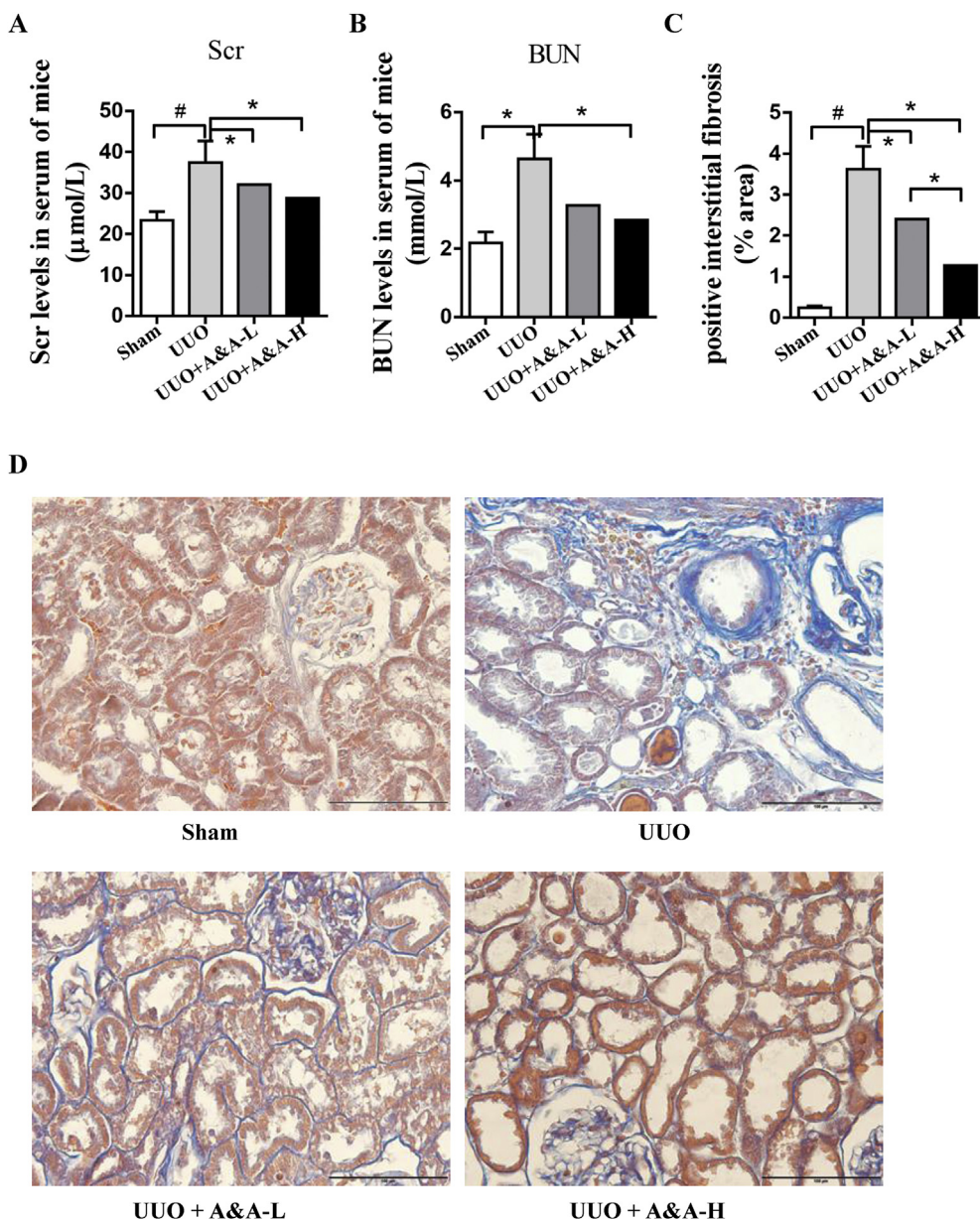
Figure 4 A&A improves renal function in mice with RIF. (A) The changes of serum SCr of kidney-injured mice in diffident groups, [#]$P < 0.01$; *$P < 0.05$ ($n = 10$). (B) The changes of serum BUN of kidney-injured mice in diffident groups, [#]$P < 0.01$; *$P < 0.05$ ($n = 10$). (C) The changes of renal histopathology in mice of different groups by Masson staining (400×). (D) Statistical analysis of positive interstitial fibrotic area in different groups, [#]$P < 0.01$; *$P < 0.05$ ($n = 10$).

kidney protection, but also reduces the number of pro-fibrotic interstitial cells.[41] TNF-α, one of the well-know proinflammatory cytokines, is implicated in the pathophysiology of numerous renal diseases.[42] TNF-α stimulates a variety of immunologically active cells when its expression is up-regulated, leading to significantly induced apoptosis of renal tubular cells.[42] Neutralization of TNF-α activity with PEG-sTNFR1 reduces the TGF-β1 expression, α-SMA accumulation, and angiotensinogen expression, thereby improving renal function after UUO. Therefore, we found that these above-mentioned signaling pathways were strictly associated with the normal renal function, and A&A could contribute to the shifting of the relative patterns of

signals about the original signaling pathways during RIF progression.

P53 is a key co-factor regulating TGF-β1-initiated transcription of pro-fibrotic genes,[43] while TGF-β1 is considered the main driver of renal fibrosis. TGF-β1 stimulates the phosphorylation of p53, promotes interactions with activated SMADs and subsequently combines with p53/SMAD3 to target promoters, involving in the process of RIF.[44] Angiotensin II (ANG II) is the primary profibrogenic factor, the effects of which are mostly associated with cell cycle dysregulation.[45] ANG II up-regulates the CCND1 expression via AT1 receptor, which dramatically stimulates profibrotic factors in collecting duct cells.[46] Studies have shown that
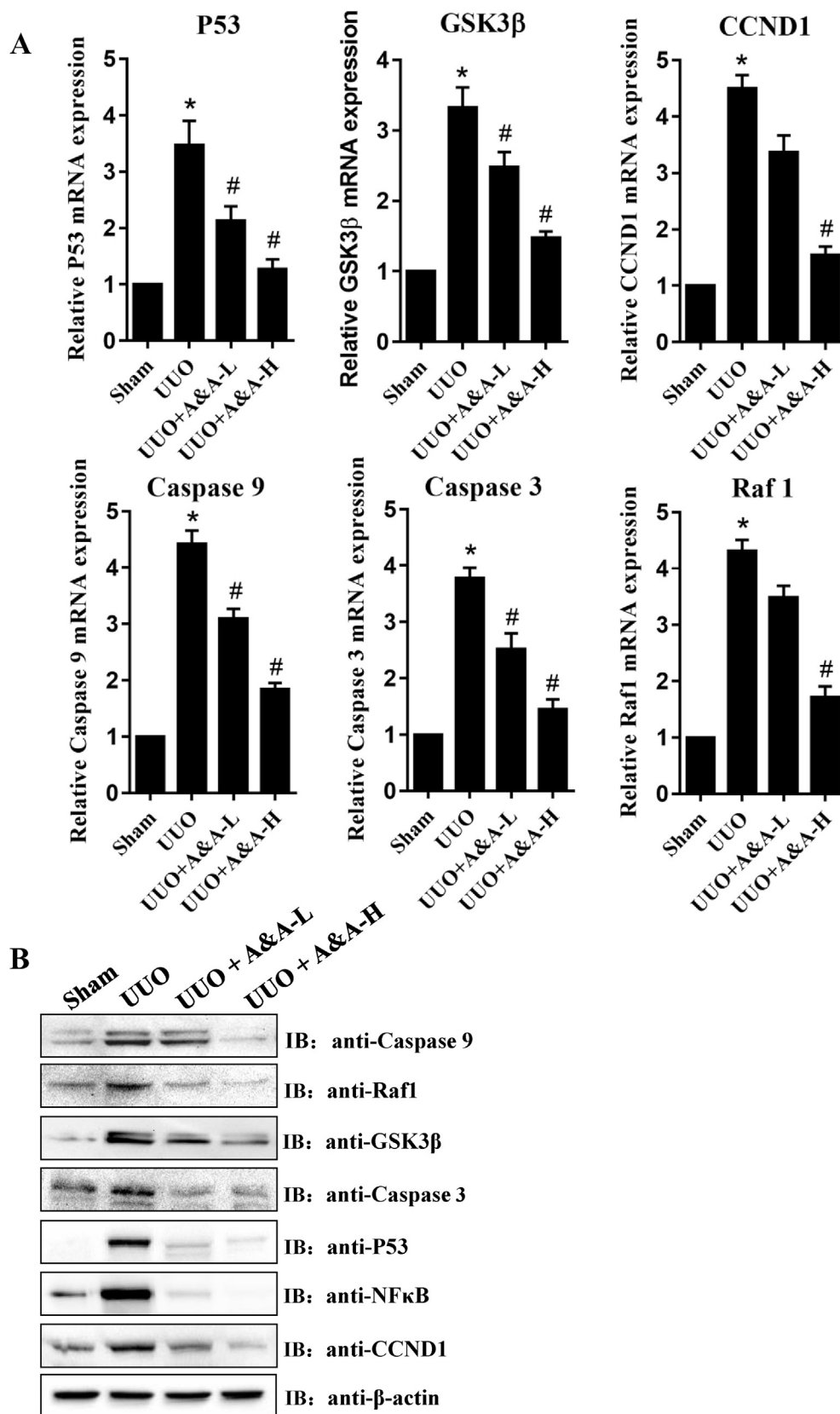
Figure 5 The expressions of core targets at the mRNA and protein levels in renal tissue. (**A**) Relative expressions of several genes at the mRNA level in the kidney of mice in different groups. (**B**) Western blotting analysis of several proteins in the kidney of mice in different groups. $^{#}P < 0.01$, compared with the sham group. $^{*}P < 0.05$ compared with the UUO group ($n = 6$).
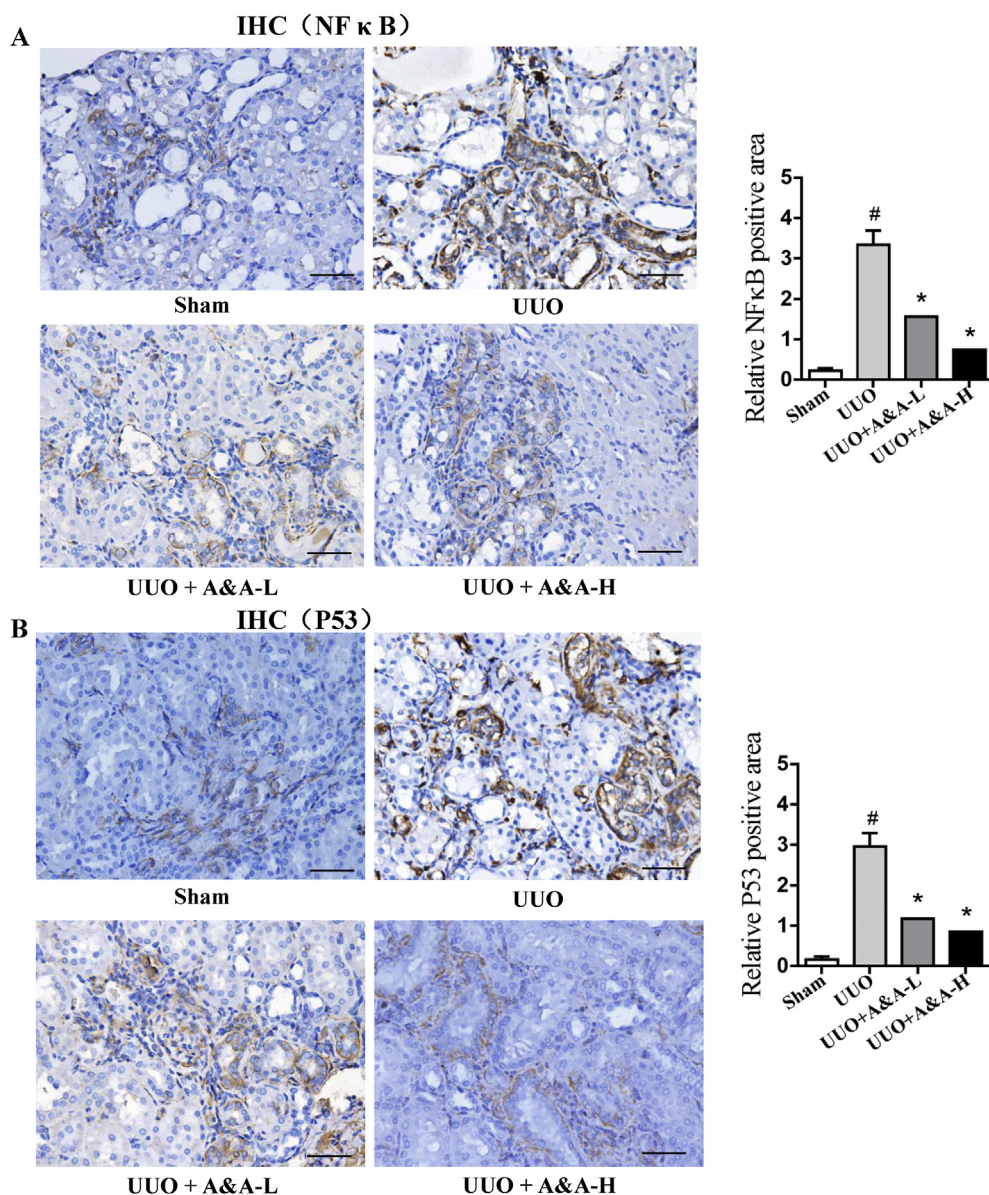
Figure 6 Expressions and immunohistochemistry analysis of NFκB and P53 in different groups. Representative immunohisto-chemistry results of NFkB (**A**) and P53 (**B**) expressions in different groups (400×). Statistical analysis of positive area was performed by Image J in different groups based on the IHC results. #$P < 0.05$ compared with the sham group. *$P < 0.05$ compared with the UUO group ($n = 10$).

EMT characterized by the changes of cell morphology and capacity has been regarded to be one of the most critical mechanisms of RIF.[47] Because RAF1 plays a vital role in the progress of EMT, it may be a potential druggable target for RIF.[48] Furthermore, evidence has shown that activated Caspase plays a key role in inflammatory reaction and apoptosis, resulting in profibrogenic and proinflammatory processes in the UUO kidneys. Previous studies have assessed the potential clinical value of Caspase 3 and Caspase 9 as therapeutic targets for the treatment of RIF.[49,50] Glycogen synthase kinase-3β (GSK3β), which belongs to the family of serine/threonine-protein kinase, can protect the renal function following renal tubular injury, and it also has been reported that GSK3 can lead to RIF via activating TGF-β signaling.[51] Above-mentioned targets identified herein might serve as potential clinical markers and play a significant role in RIF progression.

Based upon network pharmacology, 22 active compounds of A&A were identified, and seven core targets were determined, namely TP53, RELA, CCND1, RAF1, CASP3, CASP9 and GSK3β, which were considered to participate in the regulation of MAPK, PI3K-Akt and TNF signaling for RIF. In addition, the altered expressions of TP53, RELA, CCND1, RAF1, CASP3, CASP9 and GSK3β after A&A treatment might ameliorate the renal fibrogenesis by regulating the cell cycle, promoting the angiogenesis, limiting the apoptosis, and inhibiting the inflammation. Collectively, our findings provided valuable insights into the therapeutic regimens for

RIF according to "multi-component, multi-target, multi-pathway" paradigm. However, the precise active components and corresponding target genes in A&A need to be better understood and further investigated.

Author contributions

HY, XLW. These authors contributed equally to this work. HY and CFY participated in the design of this study. HY performed the network pharmacological analysis and the statistical analysis. XLW performed the in vivo experiment. XMW carried out the study and collected important background information. HY and XLW drafted the manuscript. All authors read and approved the final manuscript.

Conflict of interests

The authors have no financial conflict of interest.

Acknowledgements

Appendix A. Supplementary data

Supplementary data to this article can be found online at https://doi.org/10.1016/j.gendis.2020.06.001.

References

1. Rizzo M, Iheanacho I, van Nooten FE, Goldsmith D. A systematic literature review on the epidemiology and economic burden of anaemia associated with chronic kidney disease. *Value Health*. 2013;16(7):A381–A382.
2. Boor P, Ostendorf T, Floege J. Renal fibrosis: novel insights into mechanisms and therapeutic targets. *Nat Rev Nephrol*. 2010;6(11):643–656.
3. Zhou QG, Zheng FL, Hou FF. Inhibition of tubulointerstitial fibrosis by pentoxifylline is associated with improvement of vascular endothelial growth factor expression. *Acta Pharmacol Sin*. 2009;30(1):98–106.
4. Liu Y. Cellular and molecular mechanisms of renal fibrosis. *Nat Rev Nephrol*. 2011;7(12):684–696.
5. McClellan WM. Epidemiology and risk factors for chronic kidney disease. *Med Clin North Am*. 2005;89(3):419–445.
6. Eddy AA, Neilson EG. Chronic kidney disease progression. *J Am Soc Nephrol*. 2006;17(11):2964–2966.
7. Meng L, Van Putten V, Qu L, et al. Altered expression of gene profiles modulated by a combination of astragali radix and angelicae sinensis radix in obstructed rat kidney. *Planta Med*. 2010;76(13):1431–1438.
8. Li M, Wang W, Xue J, Gu Y, Lin S. Meta-analysis of the clinical value of Astragalus membranaceus in diabetic nephropathy. *J Ethnopharmacol*. 2011;133(2):412–419.
9. Zhong Y, Deng Y, Chen Y, Chuang PY, Cijiang He J. Therapeutic use of traditional Chinese herbal medications for chronic kidney diseases. *Kidney Int*. 2013;84(6):1108–1118.
10. Cai Q, Li X, Wang H. Astragali and Angelica protect the kidney against ischemia and reperfusion injury and accelerate recovery. *Chin Med J (Engl)*. 2001;114(2):119–123.
11. Wang H, Li J, Yu L, Zhao Y, Ding W. Antifibrotic effect of the Chinese herbs, Astragalus mongholicus and Angelica sinensis, in a rat model of chronic puromycin aminonucleoside nephrosis. *Life Sci*. 2004;74(13):1645–1658.
12. Song J, Meng L, Li S, Qu L, Li X. A combination of Chinese herbs, Astragalus membranaceus var. mongholicus and Angelica sinensis, improved renal microvascular insufficiency in 5/6 nephrectomized rats. *Vascul Pharmacol*. 2009;50(5-6):185–193.
13. Meng L, Qu L, Tang J, Cai SQ, Wang H, Li X. A combination of Chinese herbs, Astragalus membranaceus var. mongholicus and Angelica sinensis, enhanced nitric oxide production in obstructed rat kidney. *Vasc Pharmacol*. 2007;47(2-3):174–183.
14. Li S, Zhang B. Traditional Chinese medicine network pharmacology: theory, methodology and application. *Chin J Nat Med*. 2013;11(2):110–120.
15. Barton HA, Pastoor TP, Baetcke K, et al. The acquisition and application of absorption, distribution, metabolism, and excretion (ADME) data in agricultural chemical safety assessments. *Crit Rev Toxicol*. 2006;36(1):9–35.
16. Ru J, Li P, Wang J, et al. TCMSP: a database of systems pharmacology for drug discovery from herbal medicines. *J Cheminform*. 2014;6:13.
17. Xu X, Zhang W, Huang C, et al. A novel chemometric method for the prediction of human oral bioavailability. *Int J Mol Sci*. 2012;13(6):6964–6982.
18. Tao W, Xu X, Wang X, et al. Network pharmacology-based prediction of the active ingredients and potential targets of Chinese herbal Radix Curcumae formula for application to cardiovascular disease. *J Ethnopharmacol*. 2013;145(1):1–10.
19. Walters JR. New advances in the molecular and cellular biology of the small intestine. *Curr Opin Gastroenterol*. 2002;18(2):161–167.
20. Stelzer G, Rosen N, Plaschkes I, et al. The GeneCards suite: from gene data mining to disease genome sequence analyses. *Curr Protoc Bioinformatics*. 2016;54:1.30.1-1.30.33.
21. Pinero J, Ramirez-Anguita JM, Sauch-Pitarch J, et al. The DisGeNET knowledge platform for disease genomics: 2019 update. *Nucleic Acids Res*. 2020;48(D1):D845–D855.
22. Yu G, Wang LG, Han Y, He QY. clusterProfiler: an R package for comparing biological themes among gene clusters. *OMICS*. 2012;16(5):284–287.
23. Zheng KY, Zhang ZX, Du CY, et al. Ferulic acid enhances the chemical and biological properties of Astragali Radix: a stimulator for danggui buxue tang, an ancient Chinese herbal decoction. *Planta Med*. 2014;80(2–3):159–164.
24. Shi X, Tang Y, Zhu H, et al. Comparative tissue distribution profiles of five major bio-active components in normal and blood deficiency rats after oral administration of Danggui Buxue Decoction by UPLC-TQ/MS. *J Pharm Biomed Anal*. 2014;88:207–215.
25. Xu LW, Shang MY, Li J, Li XM, Meng LQ, Cai SQ. [Analysis of principal composition of ethyl acetate part in Huangqi Danggui decoction by HPLC-ESI-TOF-MS]. *Zhongguo Zhong Yao Za Zhi*. 2008;33(21):2508–2512.
26. Tang R, Zhang Y, Chen Y, Jiang L, Deng C, Zou L. Effect of different compatibility on five chemical components in Astragali Radix-Angelicae Sinensis radix. *Chin J Exp Tradit Med Formulae*. 2016;22(23):1–5.
27. Feng S, Dai Z, Liu A, et al. beta-Sitosterol and stigmasterol ameliorate dextran sulfate sodium-induced colitis in mice fed a

high fat Western-style diet. *Food Funct*. 2017;8(11): 4179—4186.

28. Park YJ, Bang IJ, Jeong MH, et al. Effects of beta-sitosterol from corn silk on TGF-beta1-induced epithelial-mesenchymal transition in lung alveolar epithelial cells. *J Agric Food Chem*. 2019;67(35):9789—9795.

29. Gabay O, Sanchez C, Salvat C, et al. Stigmasterol: a phytosterol with potential anti-osteoarthritic properties. *Osteoarthritis Cartilage*. 2010;18(1):106—116.

30. Kim GJ, Song DH, Yoo HS, Chung KH, Lee KJ, An JH. Hederagenin supplementation alleviates the pro-inflammatory and apoptotic response to alcohol in rats. *Nutrients*. 2017;9(1):41.

31. Li Y, Chi G, Shen B, Tian Y, Feng H. Isorhamnetin ameliorates LPS-induced inflammatory response through downregulation of NF-kappaB signaling. *Inflammation*. 2016;39(4):1291—1301.

32. Ohkawara S, Okuma Y, Uehara T, Yamagishi T, Nomura Y. Astrapterocarpan isolated from Astragalus membranaceus inhibits proliferation of vascular smooth muscle cells. *Eur J Pharmacol*. 2005;525(1-3):41—47.

33. Cho IA, Kim TH, Lim H, et al. Formononetin antagonizes the interleukin-1beta-induced catabolic effects through suppressing inflammation in primary rat chondrocytes. *Inflammation*. 2019;42(4):1426—1440.

34. Zhang YY, Tan RZ, Zhang XQ, Yu Y, Yu C. Calycosin ameliorates diabetes-induced renal inflammation via the NF-kappaB pathway in vitro and in vivo. *Med Sci Monit*. 2019;25: 1671—1678.

35. Liu Y, Gao L, Guo S, et al. Kaempferol alleviates Angiotensin II-induced cardiac dysfunction and interstitial fibrosis in mice. *Cell Physiol Biochem*. 2017;43(6):2253—2263.

36. Bhaskar S, Sudhakaran PR, Helen A. Quercetin attenuates atherosclerotic inflammation and adhesion molecule expression by modulating TLR-NF-kappaB signaling pathway. *Cell Immunol*. 2016;310:131—140.

37. Li X, Zhang ZL, Wang HF. Fusaric acid (FA) protects heart failure induced by isoproterenol (ISP) in mice through fibrosis prevention via TGF-beta1/SMADs and PI3K/AKT signaling pathways. *Biomed Pharmacother*. 2017;93:130—145.

38. Tamada S, Asai T, Kuwabara N, et al. Molecular mechanisms and therapeutic strategies of chronic renal injury: the role of nuclear factor kappaB activation in the development of renal fibrosis. *J Pharmacol Sci*. 2006;100(1):17—21.

39. Hers I, Vincent EE, Tavare JM. Akt signalling in health and disease. *Cell Signal*. 2011;23(10):1515—1527.

40. Winbanks CE, Grimwood L, Gasser A, Darby IA, Hewitson TD, Becker GJ. Role of the phosphatidylinositol 3-kinase and mTOR pathways in the regulation of renal fibroblast function and differentiation. *Int J Biochem Cell Biol*. 2007;39(1):206—219.

41. Liang Y, Jing Z, Deng H, et al. Soluble epoxide hydrolase inhibition ameliorates proteinuria-induced epithelial-mesenchymal transition by regulating the PI3K-Akt-GSK-3beta signaling pathway. *Biochem Biophys Res Commun*. 2015;463(1-2):70—75.

42. Meldrum KK, Meldrum DR, Hile KL, et al. p38 MAPK mediates renal tubular cell TNF-alpha production and TNF-alpha-dependent apoptosis during simulated ischemia. *Am J Physiol Cell Physiol*. 2001;281(2):C563—C570.

43. Samarakoon R, Dobberfuhl AD, Cooley C, et al. Induction of renal fibrotic genes by TGF-beta1 requires EGFR activation, p53 and reactive oxygen species. *Cell Signal*. 2013;25(11): 2198—2209.

44. Higgins SP, Tang Y, Higgins CE, et al. TGF-beta1/p53 signaling in renal fibrogenesis. *Cell Signal*. 2018;43:1—10.

45. Wolf G, Wenzel UO. Angiotensin II and cell cycle regulation. *Hypertension*. 2004;43(4):693—698.

46. Cuevas CA, Gonzalez AA, Inestrosa NC, Vio CP, Prieto MC. Angiotensin II increases fibronectin and collagen I through the beta-catenin-dependent signaling in mouse collecting duct cells. *Am J Physiol Renal Physiol*. 2015;308(4):F358—F365.

47. Liu Y. New insights into epithelial-mesenchymal transition in kidney fibrosis. *J Am Soc Nephrol*. 2010;21(2):212—222.

48. Feng D, Sheng-Dong L, Tong W, Zhen-Xian D. O-GlcNAcylation of RAF1 increases its stabilization and induces the renal fibrosis. *Biochim Biophys Acta Mol Basis Dis*. 2020;1866(3): 165556.

49. Al-Ghamdi SS, Raftery MJ, Yaqoob MM. Organic solvent-induced proximal tubular cell apoptosis via caspase-9 activation. *Environ Toxicol Pharmacol*. 2004;16(3):147—152.

50. Yang B, El Nahas AM, Thomas GL, et al. Caspase-3 and apoptosis in experimental chronic renal scarring. *Kidney Int*. 2001;60(5):1765—1776.

51. Singh SP, Tao S, Fields TA, Webb S, Harris RC, Rao R. Glycogen synthase kinase-3 inhibition attenuates fibroblast activation and development of fibrosis following renal ischemia-reperfusion in mice. *Dis Model Mech*. 2015;8(8):931—940.